Variable Stiffness Spring Actuators for Low-Energy-Cost Human Augmentation

David J. Braun, *Member, IEEE*, Vincent Chalvet, Tze-Hao Chong, Salil S. Apte, and Neville Hogan

***Abstract*—Theoretical studies suggest and experimental evidence confirms that maintaining and changing human joint stiffness by coactivated antagonistic muscles are metabolically expensive, even if muscles do not perform net mechanical work. Based on this observation, we posit that effective human augmentation can be achieved by actuators operated in parallel to human joints, even if these actuators only supplement joint stiffness without doing net mechanical work. In this article, we present a prototype variable-length leaf-spring actuator capable of large-range stiffness modulation. The key feature of the actuator is that it provides intrinsically low-energy-cost stiffness modulation even for large output deflection, by keeping the force on the driving motor low. Variable stiffness actuators use two motors to provide both stiffness and equilibrium position modulation as they are designed to do net mechanical work. The proposed actuator conceptually differs from variable stiffness actuators because first, it uses a single motor to only provide stiffness modulation, second, it does not provide equilibrium position modulation, and third, unless externally loaded, it cannot do net mechanical work. Using this actuator, we demonstrate stiffness augmentation during human–machine collaboration in challenging postural stabilization and weight-bearing tasks. Our results indicate that the proposed actuator can be used to complement a biological system by restoring or extending its functionality with low energy cost, and that variable stiffness spring actuators could effectively augment humans by doing no or a limited amount of mechanical work.**

***Index Terms*—Compliant joint/mechanism, human performance augmentation, mechanism design, physical human-robot interaction.**

Manuscript received May 4, 2018; accepted June 21, 2019. This article was recommended for publication by Associate Editor K.-J. Cho and Editor A. Kheddar upon evaluation of the reviewers' comments. This work was supported by the SUTD-MIT International Design Center as part of the Energy-Efficient Compliant Actuator Designs Project (IDG31400108) provided to D.J.B, N.H. was supported in part by NSF-NRI 1637824. This paper was presented at the IEEE International Conference on Robotics and Automation, Stockholm, Sweden, May 2016. *(Corresponding author: David J. Braun.)*

D. J. Braun is with the Department of Mechanical Engineering, Vanderbilt University, Nashville, TN 37212 USA (e-mail: david.braun@vanderbilt.edu).

V. Chalvet is with the École Nationale Supérieure de Techniques Avancées, ENSTA Paris, 91762 Palaiseau, France (e-mail: vincent.chalvet@ensta-paris.fr).

T.-H. Chong is with the Open Source Robotics Corporation Singapore Pte. Ltd. 3 Fusionopolis Way, Symbiosis, #13–21, 138633, Singapore (e-mail: aaron@openrobotics.org).

S. S. Apte is with the Ecole Polytechnique Fédérale de Lausanne EPFL, 1015 Lausanne, Switzerland (e-mail: salil.apte@epfl.ch).

N. Hogan is with the Department of Mechanical Engineering and the Department of Brain and Cognitive Sciences, Massachusetts Institute of Technology, Cambridge, MA 02139 USA (e-mail: neville@mit.edu).

Color versions of one or more of the figures in this article are available online at http://ieeexplore.ieee.org.

Digital Object Identifier 10.1109/TRO.2019.2929686

I. Introduction

DESIGNING artificial systems capable of human augmentation at a low energy cost may have significant impact on emerging areas of robotics. Recent studies have demonstrated such capability using unpowered passive exoskeletons [1], and active exoskeletons with off-board power [2]. Because humans modulate limb mechanical stiffness during functional tasks, stiffness modulation will likely prove crucial to further advances in human augmentation [3]–[5]. In this article, we show that it may be possible to realize effective human augmentation using conceptually simple variable stiffness spring actuators designed to provide large-range stiffness modulation with low energy cost.

A biologically inspired means to realize stiffness modulation is through the principle of antagonistic actuation [6]–[9]. A typical antagonistic actuator employs two motors to modulate the equilibrium position and the stiffness of a robot joint, analogous to how biceps and triceps muscles move the limb and modulate the stiffness of the elbow joint. Previous studies have shown that humans are able to modulate the stiffness of their joints, and that, in tasks involving unstable dynamics, stiffness modulation is essential [10]–[12]. It has also been pointed out that stiffness modulation is instrumental for stable robot– environment interaction [13], vital to realize safe human–robot collaboration [14], and can be exploited to achieve dynamic behavior [15], [16]. However, stiffness modulation via antagonistic actuation is energetically expensive [10], and a similar argument carries over to spring-pretension-based variable stiffness actuators [17] used to control artificial systems.

The energy required by a variable stiffness actuator is composed of the energy required to do net mechanical work, and the energy required to hold and modulate stiffness without doing net mechanical work [18]. Variable stiffness actuators typically involve at least one large motor that does most of the mechanical work via equilibrium position modulation, and one small motor responsible for stiffness modulation, which may only do a limited amount of mechanical work [19]–[21]. Using two motors, variable stiffness actuators can augment humans by providing mechanical work instead of the human. However, recent research suggests that effective human augmentation may not necessarily require an actuator capable of providing net mechanical work. This has been shown not only in zero output work tasks, such as walking [1], running [22], and squatting [23], but also in a nonzero output work task [24]. In the latter work, the authors have theoretically shown that an actuator that could only provide stiffness modulation could enable a human to accumulate kinetic

energy to move faster and jump higher beyond the natural capability of the biological limb. Therefore, it may be promising to develop conceptually simple variable stiffness spring actuators, which discard the large motor typically used for equilibrium position modulation, while retaining the small motor to provide large-range and low-energy-cost stiffness modulation.

In this article, we present a novel variable-length leaf-spring actuator, which is designed to provide stiffness modulation with low energy cost [25]. The actuator is an active spring that can change stiffness, store energy, provide force, and do mechanical work by increasing stiffness upon deflection, while it does not provide equilibrium position modulation. The key feature of the actuator is that it enables large output deflections for limited spring deflections, thereby, providing low-energy-cost stiffness modulation by keeping the force on the driving motor low [23], [26]–[28]. This feature makes it possible to render a large range of stiffness modulation at a low energy cost, not only when the actuator is near to its equilibrium configuration [17], [29]–[32], but also when it is considerably deflected from its equilibrium configuration [18]. Such variable stiffness spring actuator can be used in parallel with human joints to reduce the metabolically expensive antagonistic muscle coactivation, even if the human does all the required mechanical work.

The variable stiffness spring actuator presented in this article does mechanical work when the spring is externally loaded and the stiffness is increased. The spring may be loaded by gravity or by an external force as the human interacts with the environment. The amount of work the actuator can do depends on the size of the driving motor and the amount of energy that can be stored by the spring. In this article, we consider human stiffness augmentation and promote the use of a small motor, which could do a limited amount of mechanical work [23]–[28]. Using the proposed actuator, we experimentally demonstrate stiffness augmentation in human–machine collaboration related to isometric postural stabilization and weight-bearing tasks. Based on our experimental results, we posit that the proposed actuation concept could be used effectively to complement a biological system, by restoring or extending its function, with low energy cost.

In our previous work [25], we presented the prototype variable stiffness leaf-spring actuator, a simple analytical model of that actuator, and reported the results of two single-subject experiments to illustrate the benefit of the actuator. In this article, we, first, reveal the utility of variable stiffness spring actuators for human augmentation, second, provide a nontrivial extension of the analytical model of the proposed leaf-spring actuator, third, present numerical predictions that illustrate the nonlinear, large-deflection behavior of the actuator, fourth, present new experiments of two different human subjects, fifth, compare the proposed actuator with state-of-the-art variable stiffness actuators, and sixth, identify recently developed actuators that belong to the class of variable stiffness spring actuators promoted in this article.

The rest of this article is organized as follows. In Section II, we investigate the energy cost of stiffness modulation in biologically inspired antagonistic actuators, and we discuss previously proposed means to reduce the energy cost by changing the design of these actuators. In Section III, we recall the features of an ideal variable stiffness spring actuator, and we present the mathematical model of our variable-length leaf-spring actuator. In Section IV, we present the practical design of the variable-length leaf-spring actuator and we experimentally characterize the energy efficiency and the energy cost of maintaining and changing the stiffness of that actuator. In Section V, we present two experiments to demonstrate the utility of the proposed actuator in human augmentation. Finally, Section VI concludes this article.

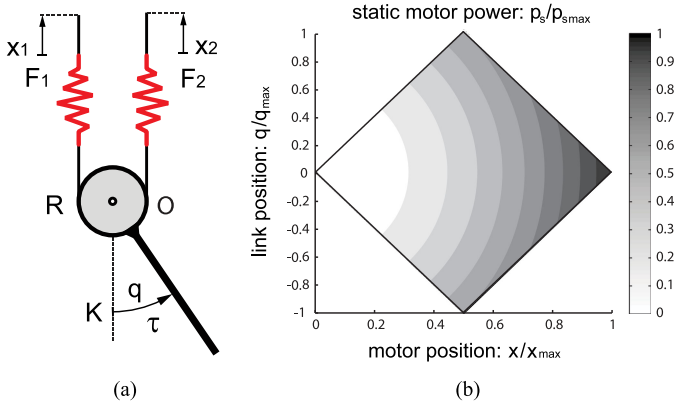

(a) (b)

Fig. 1. (a) Model of the antagonistic actuator. (b) Power required to hold a constant stiffness $K \propto x = x_1 = x_2$ for a backdrivable antagonistic actuator where $q_{\max} = \pi/2$ and $x_{\max} = R\pi$. At the equilibrium configuration, the static power is an increasing function of stiffness: $p_{\mathrm{s}}^{\mathrm{F/B}} \propto K^4 \propto x^4$.

II. Stiffness Modulation

In the human musculoskeletal system, antagonistic muscle groups enable stiffness modulation around the joints. A minimalistic model of this "biological actuator" is shown in Fig. 1(a). In this model, two motors are connected in series with two nonlinear springs, which have quadratic force–displacement characteristics [6], [8]. The joint stiffness K, equilibrium position q_0, joint torque τ, and forces imposed on the motor $\mathbf{F} = [F_1, F_2]$ are given by the following relations:

$$K = 2\kappa R^2 (x_1 + x_2), \quad q_0 = \frac{x_2 - x_1}{2R} \tag{1}$$

$$\tau = -K(q - q_0) \tag{2}$$

$$\mathbf{F} = -\kappa R^2 \left[\left(\frac{K}{4\kappa R^3} + q - q_0 \right)^2, \left(\frac{K}{4\kappa R^3} - q + q_0 \right)^2 \right] \tag{3}$$

where $q \in [-\pi/2, +\pi/2]$ denotes the link position, $(x_1, x_2) \in [0, x_{\max}] \times [0, x_{\max}]$ denote the motor positions, κ is the proportionality constant in the quadratic force–deflection relation of the springs while R denotes the radius of the pulley as shown in Fig. 1(a). When the link is displaced from its equilibrium position, restoring joint torque is generated. When the motors are simultaneously activated, both the stiffness and equilibrium position of the joint are changed.

In order to hold a nonzero stiffness, the motors are required to continuously provide a force to counteract the springs. The corresponding static electrical motor power is given by the following:

$$p_{\mathrm{s}}^{\mathrm{F}} = \frac{1}{\eta_{\mathrm{F}}^2}\frac{R_{\mathrm{m}}}{n^2 k_{\mathrm{m}}^2}\|\mathbf{F}\|_2^2 \quad \text{and} \quad p_{\mathrm{s}}^{\mathrm{B}} = \eta_{\mathrm{B}}^2\frac{R_{\mathrm{m}}}{n^2 k_{\mathrm{m}}^2}\|\mathbf{F}\|_2^2 \qquad (4)$$

where k_{m} is the motor torque constant, R_{m} is the winding resistance, n is the transmission ratio, while $\eta_{\mathrm{F/B}}$ is the forward (F) or backward (B) efficiency.[1] The distribution of this power associated with holding a constant stiffness over the entire workspace of a typical backdrivable antagonistic actuator is shown in Fig. 1(b). This plot captures the intrinsic feature of the antagonistic actuation principle, which implies that holding a constant stiffness leads to constant power drain. Below, we buttress this argument assuming that the actuator is implemented using an alternative nonbackdrivable, possibly clutched-type drivetrain. The discussion below extends to spring-pretension-based actuators [6]–[9], [33], [34], and variable moment arm actuators [17], [29]–[32], [35], [36].

A. Nonbackdrivable Drivetrain

Nonbackdrivable drivetrains, for example, worm gears and lead screws, have previously been used in spring-pretension-based antagonistic actuators [6] and variable moment arm actuators [17]. A nonbackdrivable drivetrain can be used to maintain stiffness at zero energy cost irrespective of the design of the actuator. This is because, the backward efficiency of a nonbackdrivable drivetrain is zero $\eta_{\mathrm{B}} = 0$, leading to zero static power in backward drive, (4) $p_{\mathrm{s}}^{\mathrm{B}} = 0$. This may be an ideal design in a task, where the primary purpose of the actuator is to maintain stiffness.

However energy is not only required to maintain stiffness, but it is also required to change stiffness, and changing stiffness efficiently requires an energy-efficient drivetrain. The minimum power to change stiffness is the power required to change stiffness quasistatically, which is the power in forward drive $p_{\mathrm{s}}^{\mathrm{F}}$ (4). Nonbackdrivable drivetrains, worm gears and lead screws, have low energy efficiency in forward drive $0 < \eta_{\mathrm{F}} \ll 0.5$. For this reason, nonbackdrivable drivetrains used in the aforementioned actuators cannot provide energy-efficient stiffness modulation irrespective of the design of the actuator.

B. Back-Drivable Drivetrain

Energy-efficient stiffness modulation may be achieved using a backdrivable drivetrain because a backdrivable drivetrain could provide high efficiency in forward drive $0.5 \ll \eta_{\mathrm{F}} < 1$. However, when the drivetrain is backdrivable, the motor has to counteract the force imposed by the spring $\mathbf{F}$. This may lead to high energy cost regardless of whether holding or changing stiffness is considered [18]. A controllable clutch could avoid this limitation by supporting the spring force instead of the driving motor [37]. However, a controllable clutch increases design complexity, which may not be required if the spring force is kept low by the design of the actuator.

Variable moment arm mechanisms [17], [29] could keep the motor force zero when the actuator is operated at its equilibrium configuration, and using such mechanism with a backdrivable drivetrain appears promising to realize both energy efficient and low-energy-cost stiffness modulation [18]. However, typical variable moment arm mechanisms have small output deflection range around their equilibrium configuration ($\pm 12^{\circ}$) [29], and may lead to infinite motor force as the stiffness increases, even if the output deflection remains within the deformation limit of the actuator [17], [18]. Therefore, it may be promising to develop novel actuators that could keep the motor force low even if the output is considerably deflected from its equilibrium configuration.

III. Actuator for Low-Energy-Cost Stiffness Modulation

An ideal variable stiffness spring actuator is characterized by compact design, large stiffness range, rapid stiffness change, no energy to hold stiffness, and an energy-efficient means of changing stiffness, even under mechanical load. Increasing stiffness under load increases the energy stored by the spring, and to do so requires external energy. Changing stiffness rapidly typically requires high power even if the spring is operated at its equilibrium configuration.

In this section, we propose a variable stiffness spring actuator that provides stiffness modulation with low energy cost. The main component of this actuator is a simple variable length leaf-spring mechanism shown in Fig. 2(a), see [25]. This mechanism is composed by the output link AB, a rigid connector link BC, a leaf spring CD, and a position controlled slider S. The spring is rigidly connected to the connector link at point C and is free at the other end D. In what follows, we first present a mathematical model of this actuator, and then summarize its theoretical features in comparison to the aforementioned ideal variable stiffness spring actuator.

A. Model of the Actuator

Using the nonlinear Bernoulli–Euler beam theory, the model of the actuator shown in Fig. 2(a) is given by the following equations:

$$\frac{x_{\mathrm{C}} - x}{L} = \int_0^{\theta_{\mathrm{C}}} \frac{\cos(\theta)d\theta}{\sqrt{f(m_{\mathrm{C}}, f_{\mathrm{C}x}, f_{\mathrm{C}y}, \theta_{\mathrm{C}}, \theta)}} \qquad (5)$$

$$\frac{y_{\mathrm{C}}}{L} = \int_0^{\theta_{\mathrm{C}}} \frac{\sin(\theta)d\theta}{\sqrt{f(m_{\mathrm{C}}, f_{\mathrm{C}x}, f_{\mathrm{C}y}, \theta_{\mathrm{C}}, \theta)}} \qquad (6)$$

where $(x_{\mathrm{C}}, y_{\mathrm{C}})$ denotes the location of the end point of the leaf spring C, θ_{C} denotes the deflection angle of the spring at point C, L is the total length of the undeformed leaf spring, $f = m_{\mathrm{C}}^2 + 2f_{\mathrm{C}x}[\cos(\theta_{\mathrm{C}}) - \cos(\theta)] + 2f_{\mathrm{C}y}[\sin(\theta_{\mathrm{C}}) - \sin(\theta)]$, and $m_{\mathrm{C}} = \frac{a}{L}[f_{\mathrm{C}y}\cos(\theta_{\mathrm{C}}) + f_{\mathrm{C}x}\sin(\theta_{\mathrm{C}})]$, where $f_{\mathrm{C}x,y} = \frac{L^2}{EI}F_{\mathrm{C}x,y}$ and $m_{\mathrm{C}} = \frac{L}{EI}M_{\mathrm{C}}$, denote the dimensionless reaction forces

[1] In forward drive (F), the motor deforms the spring such that the power flows from the motor into the spring. In backward drive (B), the spring helps the motion of the motor, such that the power flows from the spring to the motor. For backdrivable actuators the forward efficiency could be as high as $\eta_{\mathrm{F}} \approx 0.9$ for planetary gears and ball screw mechanism, while the backward efficiencies is approximately the same as the forward efficiency $\eta_{\mathrm{B}} \approx \eta_{\mathrm{F}}$. For nonbackdrivable worm gear and lead screw mechanisms the forward efficiency is limited to $0 < \eta_{\mathrm{F}} \leq 0.5$, while the backward efficiency is $\eta_{\mathrm{B}} = 0$.

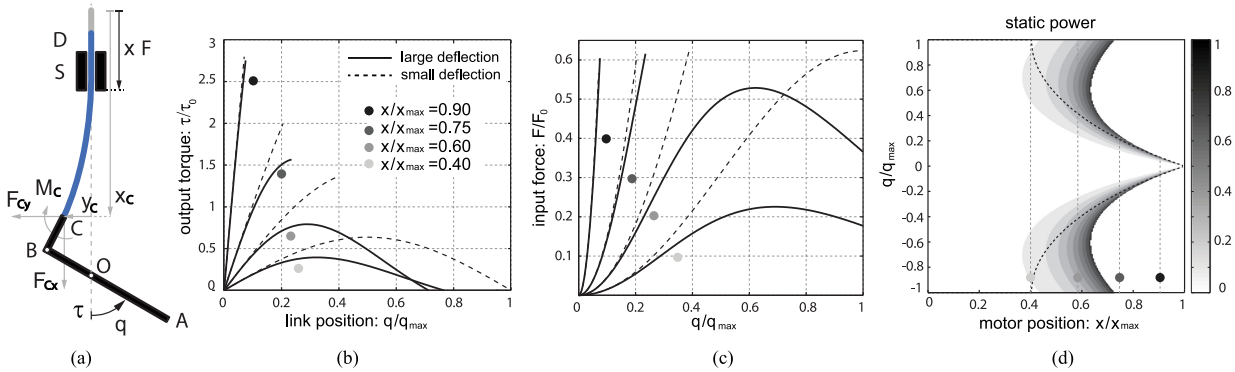

Fig. 2. (a) Model of the actuator. The blue line CD denotes the leaf spring. The two black lines, AB and BC, denote rigid links connected with a hinge joint. q is the output angle, τ is the output torque, x is the input slider position, while F is the input force exerted by the motor to the slider. (b) Output force–deflection relation of the actuator, where $\tau_0 = EIe/L^2$. (c) Input force–deflection relation, where $F_0 = EI/L^2$. In both of these plots, the solid black lines denote the predictions of the nonlinear model while the dashed black lines denote the prediction of the approximate analytical model. The approximate analytical model is only valid under small deflections i.e., when $q \in [0, \pi/10]$ rad. (d) Static power required to hold a given stiffness setting.

and the reaction moment at point C, respectively, E is Young's modulus while I is the area moment of inertia of the leaf spring.

In addition to (5) and (6), the following geometric constraints define the design of the actuator:

$$\frac{x_{\mathrm{C}}}{L} = 1 + \frac{e}{L}[1 - \cos(q)] + \frac{a}{L}[1 - \cos(\theta_{\mathrm{C}})] \tag{7}$$

$$\frac{y_{\mathrm{C}}}{L} = \frac{e}{L}\sin(q) - \frac{a}{L}\sin(\theta_{\mathrm{C}}) \tag{8}$$

where q is the link position, x is the motor position while $e = \mathrm{OB}$ and $a = \mathrm{BC}$ are the lengths of the lever arms connecting the spring to the output link, see Fig. 2(a).

Finally, the axial force $f_{\mathrm{C}x}$ is defined by the following equation:

$$f_{\mathrm{C}x} = -\frac{1}{2}m^2 = -\frac{1}{2}\left(m_{\mathrm{C}} + f_{\mathrm{C}y}\frac{(x_{\mathrm{C}} - x)}{L} - f_{\mathrm{C}x}\frac{y_{\mathrm{C}}}{L}\right)^2 \tag{9}$$

where $m = \frac{L}{EI}M$ denotes the dimensionless reaction moment of the slider S (see Appendix). Given $f_{\mathrm{C}y}$ and m_{C}, it is possible to determine $f_{\mathrm{C}x}$ from this relation. This force is the one imposed by the elastic element to the motor unit. It may seem that this force is zero because the end of the leaf spring D is free to move axially [see Fig. 1(a)]. Despite this freedom in motion, $f_{\mathrm{C}x}$ is not zero when the spring is deflected.

Using (5)–(9), one can numerically compute the output torque of the actuator as a function of the link angle q and the motor position x

$$\tau(q, x) = \frac{EIe}{L^2}[f_{\mathrm{C}x}(q, x)\sin(q) + f_{\mathrm{C}y}(q, x)\cos(q)]. \tag{10}$$

Fig. 2(b) shows this torque as a function of the output deflection for different slider positions (solid black lines). The output stiffness $K(q, x) = -\partial\tau(q, x)/\partial q$ can also be directly computed from this relation. Finally, the input force $F(q, x) = \frac{EI}{L^2}f_{\mathrm{C}x}(q, x)$, where $f_{\mathrm{C}x}(q, x)$ can be numerically computed using (9). This force is shown in Fig. 2(c).

The workspace of this actuator $(q, x) \in \mathcal{S} \subset \mathbb{R}^2$ is defined by the geometric deflection limit of the output link, the range limit imposed on the slider position, and the stress limit of the leaf spring

$$\mathcal{S} = \{(q, x) \in (-\pi/2, \pi/2) \times [0, L] : |\sigma_{\max}(q, x)| \leq \sigma_Y\} \tag{11}$$

where $\sigma_{\max}(q, x) = \frac{Eh}{2L}[m_{\mathrm{C}} + f_{\mathrm{C}y}\frac{(x_{\mathrm{C}} - x)}{L} - f_{\mathrm{C}x}\frac{y_{\mathrm{C}}}{L}]$ denotes the maximal stress in the leaf spring, while σ_Y is the yield stress. The curves in Fig. 2(b) and (c) satisfy these physical constraints.

The nonlinear model presented above accounts for many of the intrinsic features of this actuator, although the numerical predictions of this model do not provide insight into the relation between the design parameters (L, e, a, I, E, σ_Y) and the input/output relations of the actuator. In order to gain such insight, we derived approximate analytical relations of the output moment, output stiffness, and the input force, assuming small output deflection, as follows:

$$\tau(q, x) = -\frac{3EIe^2}{L^3}\frac{\cos q \sin q}{\left(\frac{a}{L} + 1 - \frac{x}{L}\right)^3 - \left(\frac{a}{L}\right)^3} \tag{12}$$

$$K(q, x) = \frac{3EIe^2}{L^3}\frac{\cos(2q)}{\left(\frac{a}{L} + 1 - \frac{x}{L}\right)^3 - \left(\frac{a}{L}\right)^3} \tag{13}$$

$$F(q, x) = -\frac{9EIe^2}{2L^4}\frac{\left(\frac{a}{L} + 1 - \frac{x}{L}\right)^2 \sin^2 q}{\left[\left(\frac{a}{L} + 1 - \frac{x}{L}\right)^3 - \left(\frac{a}{L}\right)^3\right]^2}. \tag{14}$$

These relations reduce to those presented in [25] when $a = \mathrm{AB} = 0$. The comparison between the numerical solution of the nonlinear model (5)–(9) [Fig. 2(b) and (c) solid lines] and the above-defined approximate analytical expressions [Fig. 2(b) and (c) dashed lines] indicate a reasonable match for small output deflections.

B. Physical Attributes of the Actuator

In this section, we aim to use the above approximate analytical model (12)–(14) to investigate the defining physical attributes of the actuator. In particular, we aim to investigate: 1) the stiffness

TABLE I
MOTION RANGE, STIFFNESS RANGE, AVERAGE TIME TO CHANGE STIFFNESS, AND AVERAGE RATE FOR CHANGING STIFFNESS FOR EXISTING ACTUATORS

Actuator[a]	**Motion range [deg]**	**Stiffness range [Nm/rad]**	**Average time to change stiffness*** **[s]**	**Average rate for changing stiffness [Nm/rad/s]**
Leaf-spring[b]	**±75**	**[10, 7800]**	**0.78**	**9990**
vsaUT-II [36][f]	**±45**	**[0.5, 100]**	–	–
Leaf-spring [35]	**±40**	**[0.7, 948]**	**0.78**	**1215**
HVSA [30]	**±30**	**[0, 120]**	**0.16**	**750**
Leaf-spring IV [41][e]	**±25**[1,3,6]	**[85, 24162]**[1], **[34, 5340]**[3], **[6, 957]**[6]	**0.55**[1], **0.72**[3], **0.48**[6]	**43774**[1], **7369**[3], **1982**[6]
AwAS-II [32][g]	**±18**	**[10, 10000]**	**2.5**	**3996**
Leaf-spring II [39][c]	**±17**	**[33, 955]**	**1.5**	**615**
Leaf-spring [29]	**±12**	**[252, 3648]**	**0.3**	**11320**
AwAS [31]	**±12**	**[30, 1500]**	**3.5**	**420**
Leaf-spring III [40][d]	**±11, ±4**	**[5, 900],[50, 1500]**	**0.79, 0.55**	**1133, 2637**
vsaUT [17]	–	–	–	–
VSA HD [20]	±60	[0.38, 8360]	0.4	20900
MACCEPA [33]	±60	[5, 110]	2.36	40.4
Leaf-spring I [38][b]	±40	[5, 360]	–	–
DLR BAVS [42]	±18.2	[3.9, 146.6]	0.014	10193
VSA CUBE [20]	±15.8	[3, 14]	0.18	61
DLR FSJ [34]	±15	[52.4, 826]	0.33	2344

[a]The highlighted line refers to the proposed variable stiffness spring actuator, which does not provide equilibrium position modulation. The bold entries denote *variable moment arm actuators* that satisfy condition (20) and provide low-energy-cost stiffness modulation. [b]Estimated from Fig. 3. [c]Taken from Section II-B. [d]Estimated from Figs. 7–10. [e]Experimental data not available, values taken from Tables II and III for Joints[1,3,6]. (The experimental data reported in Figs. 3 and 4 for Joint[6] show ±15° motion range and [6,60] N·m/rad stiffness range.) [f]Estimated from Figs. 17 and 18. [g]Estimated from Fig. 10. (−) data not reported. *The average time to change stiffness from minimum to maximum is not comparable between actuators because the minimum and the maximum stiffness is different for each actuator.

range; 2) the speed of stiffness modulation; 3) the motion range, and 4) the motor force required to hold stiffness of this actuator.

The summary of this investigation is provided below:

1) Stiffness Range: The output stiffness of the actuator can be modulated over a large range by changing the effective length of the leaf spring. This may be exemplified by the stiffness range at equilibrium

$$K(0,x) \in [K_{\min}, K_{\max}) = \left[\frac{3EIe^2}{L^3}\frac{1}{\left(\frac{a}{L}+1\right)^3-\left(\frac{a}{L}\right)^3}, \infty\right). \tag{15}$$

Consequently, the output link becomes rigidly connected to the frame of the actuator, which means infinite stiffness $\lim_{x\to L} K(0,x) = K_{\max} \to \infty$. On the other hand, the actuator cannot achieve zero stiffness. Nevertheless, the minimum stiffness can be low i.e., $\lim_{x\to 0} K(0,x) = K_{\min} \propto e^2 L^{-3}$ when $0 < e/L \ll 1$, leading to almost free motion [Table I and Fig. 5(e)]. Also, due to the inverse relation between the minimum stiffness and the length of the spring, low stiffness can be afforded by a relatively compact actuator.

We note that infinite stiffness range may require an infinitely large antagonistic actuator (see Fig. 1), because the stiffness is quadratically related to the size of that actuator $K \propto R^2$ and linearly related to the average displacement of the motors $K \propto \frac{1}{2}(x_1 + x_2)$ (1). The same limitations extend to spring-pretension-based actuators [6]–[9], [33], [34], and some variable moment arm actuators [31] i.e., they are not capable of infinite-range stiffness modulation. Nevertheless, there are previously designed variable moment arm actuators that are theoretically capable of infinite stiffness [17], [23], [25], [29], [38]–[41] and zero stiffness [32], [35], [36], and even negative stiffness is achievable by a nontrivial modification of the proposed actuator [27], [28]. The stiffness range for a number of previously designed actuators is provided in Table I.

2) Speed of Stiffness Modulation: The speed of stiffness modulation at the equilibrium configuration is defined by the following relation:

$$\frac{dK(0,x)}{dt} = \frac{dK(0,x)}{dx}\frac{dx}{dt} \tag{16}$$

where the first term on the right-hand side depends on the design of the actuator, while the second term $\dot{x} = dx/dt$ is the speed of the motor. For the proposed actuator, the relation between the stiffness and the motor position is given by the following:

$$\frac{dK(0,x)}{dx} = \frac{9EIe^2}{L^4}\frac{\left(\frac{a}{L}+1-\frac{x}{L}\right)^2}{\left[\left(\frac{a}{L}+1-\frac{x}{L}\right)^3-\left(\frac{a}{L}\right)^3\right]^2}. \tag{17}$$

According to (17), the speed of stiffness modulation tends to infinity at high stiffness settings

$$\lim_{x\to L}\frac{dK(0,x)}{dt} \to \infty. \tag{18}$$

Consequently, the actuator can be used for fast stiffness modulation at large stiffness $K|_{x\approx L} \approx K_{\max}$, even if the speed of the motor is limited $|\dot{x}| \le \dot{x}_{\max}$. This is due to the nonlinear motor position versus output stiffness relation (17), which enables large stiffness changes using small changes in motor position. We use this feature to demonstrate fast stiffness modulation at large stiffness using a relatively slow motor [Table I and Fig. 5(e)]. The same feature may also enable fast stiffness modulation in previously designed actuators [17], [27], [32], [36], while it does not apply in spring-pretension-based actuators [6]–[9], [33], [34]. For example, in antagonistic actuators with quadratic springs [6], [7], the speed at which stiffness can change is

$dK/dt|_{x=x_1=x_2} = 4\kappa R^2 \dot{x}$, which means that fast stiffness modulation requires a fast motor $|\dot{x}| \leq \dot{x}_{\max} \to \infty$ or a large actuator $R \to \infty$. The speed of stiffness modulation for a number of previously designed actuators is provided in Table I.

3) Motion Range: The motion range of the actuator is limited by its geometric design, and the deformation limit of the leaf spring. These limitations are represented by the following constraint:

$$|\sin q| \leq \min \left\{ 1, \frac{2}{3}\frac{\sigma_y}{E}\frac{L}{h}\frac{L}{e}\frac{(\frac{a}{L}+1-\frac{x}{L})^3-(\frac{a}{L})^3}{\frac{a}{L}+1-\frac{x}{L}} \right\} \quad (19)$$

where h is the thickness of the spring. Consequently, the theoretical motion range of the mechanism may extend to $q \in (-\pi/2, +\pi/2)$, when the stiffness is below a certain finite value $0 \leq x \leq x_{\text{cr}} \in [0, L]$.[2] This allows a relatively large output deflection (Section IV Fig. 4) compared to most variable stiffness actuators [17], [29]–[32], [35].

When the stiffness is higher than the critical value (i.e., $0 \leq x_{\text{cr}} < x \in [0, L]$), the motion range of the output link is limited by the stress limit of the leaf spring: $|\sin q| \leq \frac{2}{3}\frac{\sigma_y}{E}\frac{L}{h}\frac{L}{e}[(\frac{a}{L}+1-\frac{x}{L})^3-(\frac{a}{L})^3]/[\frac{a}{L}+1-\frac{x}{L}]$. According to this inequality relation, the motion range shrinks down to zero as the stiffness approaches infinity ($x \to L$). This physical limitation is fundamental in the sense that it applies to actuators capable of infinite-range stiffness modulation. The elastic deflection range for a number of previously designed actuators is provided in Table I.

4) Motor Force: The force required by the motor to hold a certain stiffness setting, fixed slider position, is zero when the actuator is not loaded externally (i.e., when the actuator operates at its natural equilibrium configuration $q = 0$), see (14)

$$F(0, x) = 0. \quad (20)$$

This feature ensures that, at the equilibrium configuration, the motor can adjust the stiffness of the actuator without being opposed by the spring. This is not the case for spring-pretension-based actuators, where the force increases with the stiffness even at the equilibrium configuration [18]. This can be seen in the biologically inspired antagonistic actuator, where $F_{1,2} \propto K^2$ even when the actuator is not deflected from its equilibrium configuration, see (1). On the other hand, (20) represents a typical feature of actuators based on the variable moment arm principle [17], [29]–[32]. Variable moment arm actuators that satisfy condition (20) are denoted with bold text in Table I.

When the actuator is externally loaded (i.e., $q \neq 0$), the static motor force F remains bounded regardless of the joint deflection and the stiffness

$$|F(q, x)| \leq \max_{(q,x)\in\mathcal{S}} |F(q, x)| = F_{\max} = \frac{\sigma_Y^2 A}{6E} < \infty \quad (21)$$

where A denotes the cross-section area of the spring. This remains true even if the actuator approaches infinite stiffness

$$\forall (q, x) \in \mathcal{S} : \lim_{x \to L} |F(q, x)| = F_{\max}. \quad (22)$$

Conditions (20) and (21) show that the proposed variable-length leaf-spring design [Fig. 2(a)] used an intrinsically low-power variable stiffness mechanism [18]. This mechanism ensures low-energy-cost stiffness modulation by keeping the force required by the driving motor low (highlighted in Table I, and Fig. 4). We posit that the combination of such intrinsically low-power mechanism with a backdrivable energy-efficient drivetrain may be used to design actuators that can provide both energy efficient and low-energy-cost stiffness modulation.

C. Discussion

Actuators enabling stiffness modulation without requiring force, and as such input power, to hold a given stiffness at their equilibrium position (20), have previously been designed [17], [29]–[32], [35]. Some of these actuators enable near zero and near-infinite stiffness, and some previously designed actuators [19] may also be used to realize high-speed stiffness modulation. However, we are not aware of an actuator that combines the four abovementioned features. For example, condition (21) is not satisfied by the stiffness modulating mechanism of many previously designed antagonistic and nonantagonistic actuators, including some variable moment arm actuators, see [18]. More generally, achieving an infinite stiffness range; low energy cost when the actuator is operated away from its equilibrium configuration; large kinematic motion range at low stiffness; and high-speed stiffness modulation at high stiffness, have been recognized as difficult to achieve within a single design. In the analysis above, we indicated how, and under what conditions, the presented actuator could fulfill these requirements.

Many of the previously designed variable moment arm actuators [17], [29]–[31] satisfy condition (20) required for low-energy-cost stiffness modulation at equilibrium, but they do not employ leaf springs. Consequently, it may appear that the use of a leaf spring leads to the defining features (15)–(22) of the proposed actuator. However, these features are not inherent to leaf-spring designs. Leaf springs have been previously used to construct nonlinear elastic elements for antagonistic actuators [43], and they have also been used as prestressed elastic elements in nonantagonistic actuators [38]. The use of leaf springs does not provide intrinsically low-energy-cost stiffness modulation partly because (20) does not hold in these actuators. This is the same reason why antagonistic actuators [6], [7], and other spring-pretension-based actuators [33], [34], do not provide intrinsically low-energy-cost stiffness modulation [18].

There are also leaf-spring actuators in which the bending stiffness is changed by changing the effective area moment of inertia of the spring. This can be done by rotating the spring along its longitudinal axis as proposed in [44]. This kind of actuator satisfies (20) although it cannot provide infinite-range stiffness modulation because the stiffness is proportional to the second area moment of the spring.

[2]The critical value of the slider position x_{cr} is defined by: $\frac{2}{3}\frac{\sigma_y}{E}\frac{L}{h}\frac{L}{e}\frac{(\frac{a}{L}+1-\frac{x_{\text{cr}}}{L})^3-(\frac{a}{L})^3}{\frac{a}{L}+1-\frac{x_{\text{cr}}}{L}} = 1$, and it exists if $\frac{2}{3}\frac{\sigma_y}{E}\frac{L}{h}\frac{L}{e}\frac{(\frac{a}{L}+1)^3-(\frac{a}{L})^3}{\frac{a}{L}+1} \geq 1$.

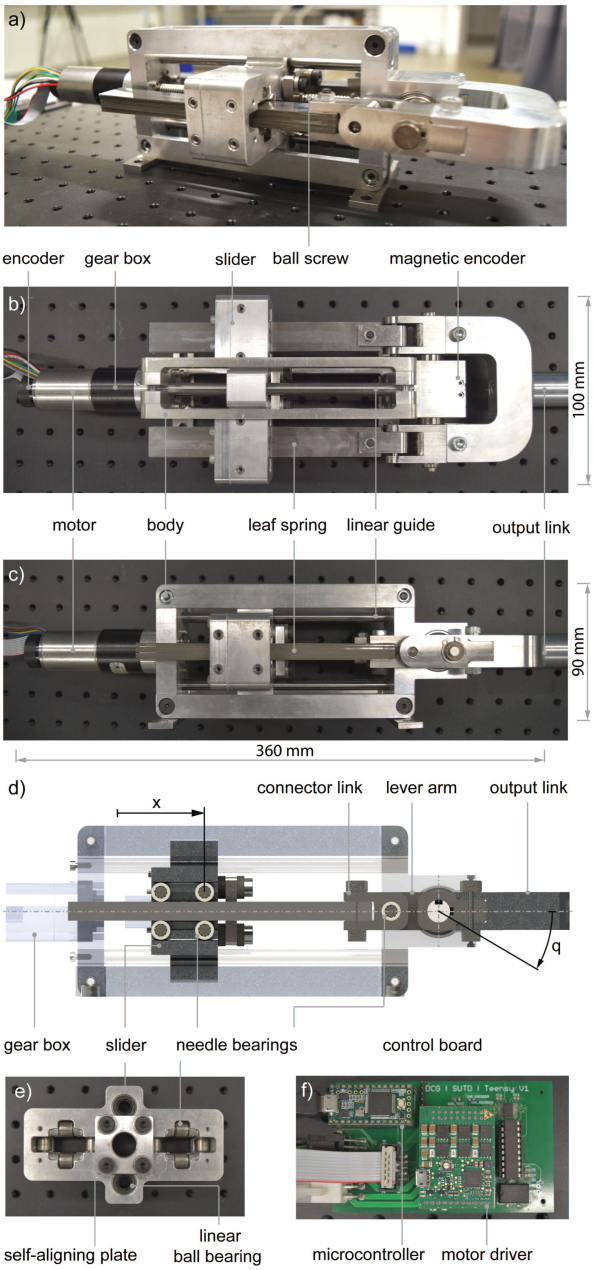

Fig. 3. (a) Bench-top prototype, (b) top view, (c) side view. (d) Model of the actuator. This model shows the practical realization of the variable-length leaf-spring design. (e) Design of the slider. (f) Electronic control board. The physical properties of this prototype are shown in Table II.

The leaf-spring design [29] provides low-energy-cost stiffness modulation within a $\pm 12^\circ$ motion range (see [29, Fig. 9]). The limited motion range is due to the rigid cantilever support used to fix the leaf spring. This is a typical design feature of previously developed leaf-spring actuators [29], [35], [39]–[41]; it leads to large internal forces in the spring even at small to moderate output deflections. The design proposed in this article uses a sliding cantilever support and a kinematic link AOB, where the spring is connected to the hinge joint B [Fig. 2(a)]. This design leads to limited spring deflection even for large output deflection, thereby keeping the force and the power drained by the driving motor low (Section IV Fig. 4). This design also alleviates motion range limitations present in previously designed variable moment arm actuators (highlighted in Table I); the large output motion range $\pm 75^\circ$ with low stiffness makes it possible to use this actuator without an extra motor dedicated to equilibrium position modulation.

TABLE II
PHYSICAL PROPERTIES OF THE VARIABLE STIFFNESS SPRING ACTUATOR

Weight[a]	3 kg
Size[a] (length × height × width)	90 × 100 × 360 mm
Motion range[b]	$\pm\mathbf{75}$ deg
Stiffness at equilibrium[c]	$[\mathbf{10, 7800}]$ Nm/rad
Average time to change stiffness[d]	0.78 s
Average rate for changing stiffness[e]	**9990** Nm/rad/s
Maximum static power[f]	**2.25** W
Dynamic power (maximum speed, no load)[f]	**8.20** W

[a] The weight and size of the prototype can be substantially reduced by design optimization; see [23], [48] and Section VI for a related discussion.
[b] $[q_{\min}, q_{\max}]$ is the output motion range at minimum stiffness.
[c] The stiffness tends to infinity as the length of the spring approaches zero, see (15). This is shown in Fig. 5(e). As the length of the spring reduces to zero, the output link becomes kinematically locked. In this case, the output stiffness is the structural stiffness of the device, and the restoring torque is limited by the torque required to break the output link.
[d] The time to decrease stiffness from maximum to minimum and to increase stiffness from minimum to maximum is shown in Fig. 5(e).
[e] The rate of decreasing and increasing stiffness is shown in Fig. 5(e). The rate of change of stiffness tends to infinity as the length of the spring reduces to zero, see (18) and Fig. 5(e).
[f] The static and dynamic power is shown in Figs. 4 and 5(f).

We note that there are at least three distinct ways a dynamical system can be actuated. The first is force or equilibrium position modulation commonly implemented using motors or series elastic actuators [45], the second is equilibrium position and stiffness modulation, which is realized by variable stiffness actuators [46], while the third is stiffness modulation [47] implemented by the proposed variable stiffness spring actuator. Previous stiffness modulating mechanisms were developed and used as subcomponents that make variable stiffness actuators out of simpler series elastic actuators. This article does away with this notion and proposes controlled stiffness modulating mechanisms as independent actuators.

IV. MECHANICAL DESIGN

A bench-top prototype has been designed and fabricated, see Fig. 3. The kinematic realization of this prototype resembles the minimalistic model shown in Fig. 2(a) with the output link, leaf spring, and the position controlled slider. The weight, size, and the shape of this device has not been optimized for portable applications, see Table II. A discussion on such optimization is deferred to Section VI. Here, we detail the mechanical design and present the experimental characterization of the actuator. Subsequently, in Section V, we use this actuator for human augmentation.

A. Design

The actuator has a rectangular body. This body houses the slider, the drivetrain, the leaf spring, and the output link. In the following, we describe these components in detail.

The slider Fig. 3(e) is used to change the effective length of two springs Fig. 3(b). The motion of the slider is supported by two 8 mm diameter linear guides made of hardened SUS440C steel. These linear guides are fixed to the body of the device as shown in Fig. 3(c). The friction between the slider and the linear guides is minimized using linear ball bearings SKF LBCR8 2LS/HV6 (see Fig. 3(e) and Section IV-B for more details). The slider is driven by a 10×2 mm Maxon ball-screw. The ball screw is actuated by a brushless dc motor (Maxon EC-max 24 V and 40 W) via a one-stage $4.8:1$ gear ratio planetary gearbox [Fig. 3(b)]. The latter three components comprise the drivetrain of the actuator. The drivetrain has a maximum electrical input to mechanical output efficiency of $\eta_{\max} = 67\%$ (according to factory specifications, the efficiency of the motor is 89%, while the efficiency of the ball screw and gearbox assembly is 75%).

The elastic element is implemented by two stacks of leaf springs connected to the output link as shown in Fig. 3(a)–(d). These composite springs, of width $b = 20$ mm, are assembled from five $n_1 = 5$, $h_1 = 1$ mm thick and nine $n_2 = 9$, $h_2 = 0.5$ mm thick full-hard AISI 301 stainless steel leaves. The yield stress of the springs is $\sigma_Y = 1250$ MPa. The torque, stiffness, and the motor force can be calculated using previously derived formulas (12)–(14), where the total area moment of inertia of the two composite leaf springs is given by the following:

$$I = \frac{b}{6}\left(n_1 h_1^3 + n_2 h_2^3\right). \tag{23}$$

According to this relation, the torque depends on the cube of the individual spring thickness. As such, by changing the thickness h_1 and h_2 of individual leaves, as well as the number of leaves n_1 and n_2, the force–deflection characteristic of the actuator can be tuned.

The leaf springs are connected to the output link via a hinge joint and a two-link mechanism. This mechanism closely resembles the kinematics of the ideal design (see Fig. 2(a) OBC). On the opposite end, the springs are interfaced with the slider via a sliding cantilever support. In order to eliminate sliding friction, the interface between the springs and the slider is realized using needle bearings SKF HK 0609 (see Fig. 3(d) and (e) and Section IV-B for more details). This connection enables the output link to undergo large deformations while keeping the deflection of the springs limited.

We use closed-loop position control to set the effective length of the leaf springs, and consequently, the stiffness of the actuator. The controller uses the actual position of the slider x provided by the motor encoder Fig. 3(b). The control board used to drive the motor is shown in Fig. 3(f). The practical implementation consist of an ARM Cortex-M4 microcontroller, a Maxon ESCON 50V/5A 4-Q motor driver used in current control mode, and a custom-made printed circuit board. The system was operated with 500 Hz sampling rate. The power drained by the motor was recorded with a dedicated power measuring circuit (TI INA219). The resolution of the power measurement was 0.025 W. The motion of the output link q was measured using a 12-b off-axis absolute magnetic position sensor (AMS, AS5045).

B. Practical Consideration

There are four practical limitations that impede exact realization of the conceptual design shown in Fig. 2(a). The first stems from the difficulty of realizing an ideal cantilever support Fig. 3(d), the second is caused by friction between the slider and the leaf springs Fig. 3(c)–(e), the third is caused by backlash at the output link, while the fourth is due to the friction between the slider and the linear guides Fig. 3(b)–(e). These practical issues were mitigated in the following way:

1) The ideal cantilever support used in the model [Fig. 2(a)] was realized by roller-cantilever support, see Fig. 3(d) and (e). This design was adapted to avoid sliding friction as discussed below. Due to the introduction of the rollers, the model (14) overestimates the motor force.
2) The roller bearings eliminate the undesirable sliding friction between the slider and the springs Fig. 3(d) and (e). Due to the introduction of the rollers, the interface between the slider and the rollers is only affected by rolling friction, which remains low even if a large normal force acts between the springs and the slider. Consequently, the normal reaction force does not lead to high frictional force and stick–slip effects in this actuator.
3) Backlash was observed at the output link when the actuator was not loaded. In order to minimize this effect, the distance between the rollers has been precisely defined to reduce the free-play of the springs [Fig. 3(d)]. Alternatively, one could make the distance between the rollers adjustable. This design could be used to eliminate the free-play between the rollers and the leaf springs.
4) Friction between the linear guides and the slider is reduced using linear ball bearings [Fig. 3(e)]. Reducing the internal friction is essential in compliant actuators. This is because friction leads to energy dissipation, which could become dominant when considering intrinsically efficient actuators. Using ball bearings and roller bearings, instead of plain bearings, one can reduce friction by reducing the coefficient of friction. However, rolling friction depends on the normal forces in the actuator, similar to how sliding friction depends on the normal force in plain bearings. Eliminating these forces is not possible, but reducing them in a way that does not affect stiffness modulation can alleviate frictional losses.

The use of prestressed springs in variable moment arm actuators leads to persistent internal forces even if the actuator is not displaced from its equilibrium configuration ($q = 0$). These internal forces make many of the previously designed variable moment arm actuators vulnerable to increased friction and increased energy cost in practical application (see [17] Section VIII). In the proposed actuator, the leaf springs are not prestressed and internal forces are only present when the output link is displaced from its equilibrium position ($q \neq 0$). When the output link is not displaced ($q = 0$), the leaf spring remains unloaded, and stiffness can be changed from near-zero to near-infinity without resulting in losses due to the increased rolling friction caused by internal forces. Indeed, the normal reaction force between the leaf spring and the slider remains zero

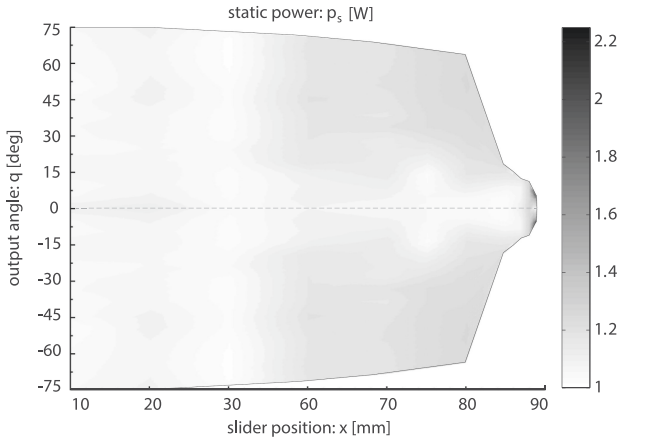

Fig. 4. Experimental data measured for $q \in [0, 75°]$ and extrapolated to $q \in [-75°, 75°]$. Static electrical motor power over the workspace of the actuator. The total power $p_s = p_0 + \Delta p$ is the sum of the baseline power $p_0 \approx 1$ W (required by the supporting electronics) and the power required to hold a given stiffness setting Δp.

in this case, regardless of the stiffness setting of the actuator, see Fig. 3(d).

C. Characterization

In this section, we report: 1) the power required by the actuator to hold stiffness under external load and no load; 2) the speed of stiffness modulation; 3) the power required to change stiffness under no external load, the power required to change stiffness and do mechanical work under external load; and 4) the energy efficiency of the actuator while changing stiffness under load.

The reported experimental data reflect all the energy losses in the actuator, including friction, which is challenging to estimate using model-based calculations.

1) Static Motor Power: Fig. 4 shows the static electrical motor power $p_s \leq 2.25$ W required to hold stiffness over the entire workspace of the actuator $(x, q) \in [0, x_{\max}] \times [q_{\min}, q_{\max}] = [0, 0.08]$ m $\times [-75, 75]°$. The plot also shows the baseline electrical power $p_0 \approx 1$ W taken by the electronics when the motor was stationary $\dot{x} = 0$, and the link was at its equilibrium configuration ($q = 0$). The data indicate a low-static mechanical power $\max \Delta p = p_s - p_0 \leq 1.25$ W in the entire workspace of this backdrivable actuator. The power remains low even when the output link is deflected from the equilibrium configuration ($q \neq 0$) and regardless of the stiffness setting. This is due to the particular way this actuator is designed, which prevents the external load from propagating to the motor. For example, Fig. 5(a) and (b) shows the behavior of the actuator under load ($\approx$5 N·m) at low- and high-stiffness settings. In both cases, the right panel of the power supply indicates the voltage (24 V) and the current (0.06 A) taken by the device. According to these readings, the total electrical power is below 1.5 W.

According to the experimental data (see Figs. 4 and 5), the mechanical power ($\leq$1.25 W) required by the actuator was nearly the baseline electrical power (1 W) drained by the minimalistic

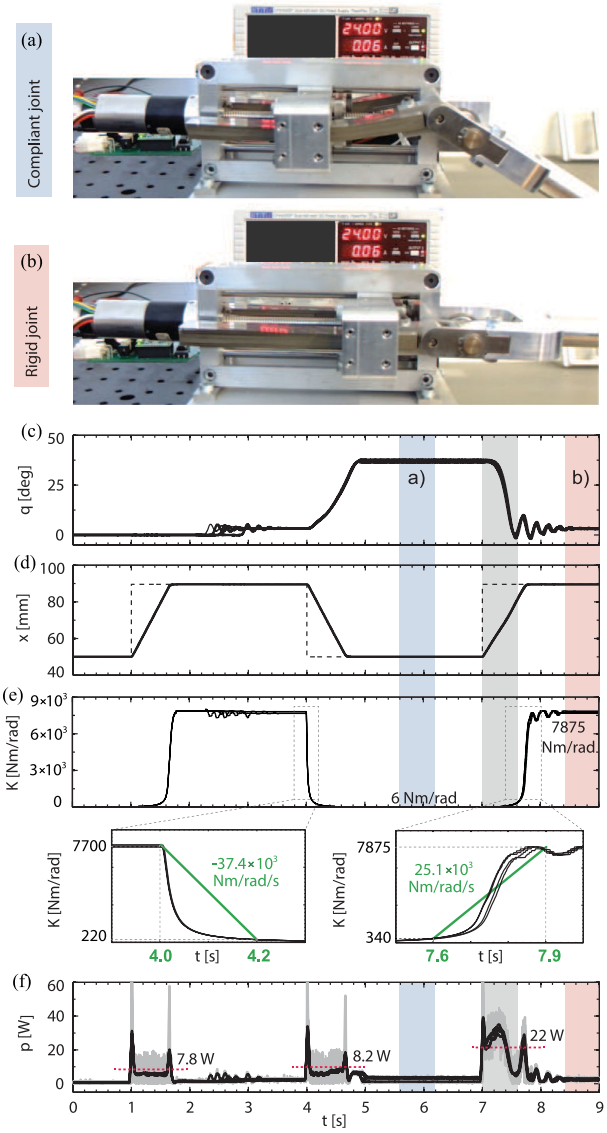

Fig. 5. Behavior of the actuator under $\approx$5 N·m external load. (a) Low-stiffness setting. (b) High stiffness setting. (c) Link angle q. (d) Slider position x (black lines), step command (dashed lines). (e) Stiffness K (13) and the rate of change of stiffness (inset). (f) Electrical power p; instantaneous power (gray lines), average power (black lines). (c)–(f) show the data of the same experiment repeated four times.

electronics and the Maxon ESCON 50/5 motor controller [see Fig. 3(f)]. Similar power consumption was previously reported for a stiffness modulating mechanism used in [31], where the output motion was limited to small angles ($\pm 12°$), as opposed to ($\pm 75°$) in the proposed actuator (see Fig. 4). We note that holding stiffness should require zero power by an ideal actuator because in this task no mechanical work is done by the actuator [18]. This theoretical limit has recently been approached by an electro-adhesive clutch spring [49]. This clutch can be used for ON–OFF type stiffness modulation when the spring is not externally loaded ($q = 0$), but since neither the clutch nor the spring can do work, the clutch spring cannot increase stiffness when externally loaded ($q \neq 0$).

2) Speed of Stiffness Modulation: Fig. 5(c) and (d) shows the behavior of the actuator under load (≈ 5 N·m) while the slider is subject to a step command. At the minimum position of the slider [see Fig. 5(a)], the stiffness of the output is low for this task ($\approx$6 N·m/rad). This is why, despite the low damping, the motion of the joint appears to be over-damped (see Fig. 5(c) $t \in [4, 5]$ s). When the position of the slider is at its maximum [see Fig. 5(b)], the stiffness is high ($\approx [7700, 7875]$ N·m/rad) and the output link is close to being rigid. In this case, the joint is under-damped and exhibits fast oscillations (see Fig. 5 $t \in [7, 10]$ s). According to Fig. 5(d), changing from minimum to maximum stiffness or vice versa is relatively slow, i.e., it requires $\approx [0.7, 0.8]$ s. This may suggest that fast stiffness modulation is not attainable. However, due to the approximate inverse square relation (17) i.e., $dK(0, x)/dx|_{x\to L} \propto (1 - x/L)^{-2}$, the stiffness can be changed rapidly (18) in high stiffness domains [see Fig. 5(e)], even if the slider moves slowly [see Fig. 5(d)]. In turn, the rapid change in stiffness results in under-damped oscillations as the output angle returns to the equilibrium position (see Fig. 5 $t \in [7, 10]$ s). A faster motor could provide faster slider motion and thus a faster overall stiffness change in this actuator. However, increasing the speed of the motor would require more power, regardless of the design of the actuator.

3) Power to Change Stiffness and do Mechanical Work: Fig. 5(e) ($t \in [1, 2]$ s and $t \in [4, 5]$ s) shows that the average electrical power ($p = p_s + \Delta p \in [7.8, 8.2]$ W) required to increase or decrease stiffness under no-load is higher than the largest static power (2.25 W). The difference between these numbers depends on the speed of the motor; it can be lower if the motor moves slower, and can be higher if the motor moves faster. Fig. 5(e) also shows that increasing stiffness under load requires power. For example, in the experiment shown in Fig. 5(e) $t \in [7, 8]$ s, the increase in stiffness generates output force. In order to generate this force, the actuator requires power (on average $p \approx$22 W). This is the electrical power required to hold stiffness, move the slider, and deform the spring. We note that this power depends on the mechanical requirement imposed by the task i.e., here it is to lift the weight [see Fig. 5(a) and (b)]. This mechanical requirement cannot be reduced. This is why a controllable clutch attached to a spring [49] that cannot do net mechanical work, would not be able to perform this task.

4) Energy Efficiency of Stiffness Modulation: Energy efficiency is defined by the ratio of the mechanical power at the actuator's output and the electrical power at its input. Factory specifications of electric motors report the largest efficiency obtained under a nominal, constant speed, operating condition. This efficiency is $\eta^{\text{mot}}_{\max} = 89\%$ for the motor used in the present actuator. However, constant speed operation is uncommon in applications, and as such a typical efficiency is considerably lower when it comes to robotic applications. For example, an energy-efficient quadrupedal robot locomotion was characterized by $\eta = 24\%$ according to a recent report [50]. This seemingly low efficiency is comparable to the maximal efficiency of a human muscle $\eta^{\text{mus}}_{\max} = 29\%$ [51].

The energy efficiency discussed above has not been reported for prior variable stiffness actuators [17], [31]. Also, this efficiency cannot be defined meaningfully when stiffness is modulated at the equilibrium position, because, in that case, the output mechanical power of the actuator is zero [18]. Nevertheless, the efficiency of stiffness modulation can be defined for a task where the actuator is externally loaded, and the stiffness is increased from a low to a high value. In this case, the efficiency is defined by the ratio of the mechanical energy output E_m and the electrical energy input E_e i.e., $\eta = (E_m/E_e) \times 100\%$. This efficiency is not the maximal efficiency of the actuator, but instead, it is the typical efficiency associated with the considered task. Also, this efficiency includes all the losses in the actuator; the energy losses in the ball screw, bearings, gearbox, motor, and the losses in the supporting electronics.

In order to calculate $\eta = (E_m/E_e) \times 100\%$, we revisit the experiment shown in Fig. 5(a) and (b) and (c)–(e) $t \in [t_0, t_1] = [7, 7.6]$ s. In this experiment, the stiffness was initially low and the output was deflected from the equilibrium $q(t_0) \approx 37^o = 0.65$ rad (see Fig. 5(c) $t_0 = 7$ s). Subsequently, the motor was used to increase the stiffness (see Fig. 5(d) $t \in [7, 7.6]$ s). Due to the increase in stiffness, the output link moved back to the equilibrium position $q(t_1) = 0$ (see Fig. 5(c) $t_1 = 7.6$ s). The electrical energy input was calculated by the integral of the measured electrical power $E_e = \int_{t_0}^{t_1} |p(t)|dt \approx 13.9$ J [see Fig. 5(e)]. The mechanical work was calculated by the negative potential energy difference between the initial and the final configuration $E_m = mgL[\sin q(t_1) - \sin q(t_0)] = 2.1 \times 9.81 \times 0.25 \sin(0.65) \approx 3.1$ J. Based on these calculations, the efficiency was estimated[3] $\eta \approx 22\%$. This efficiency is similar to the previously reported typical efficiency for state-of-the-art quadrupedal walking robots (24% [50]), and is comparable to the maximal efficiency of human muscles (29% [51]). With further design optimization [52], we foresee higher efficiency achievable with this actuator.

V. Stiffness Augmentation

In various natural tasks, including standing and locomotion, weight-bearing, and postural stabilization are vital. Closed-loop force control and open-loop stiffness control are both viable approaches to achieve these tasks. Humans are able to utilize both of these control modalities, and it has been shown [12] that they may prefer one over the other, depending on the control task.

It has been previously argued that the ability of humans to cope with challenging stabilization tasks, under inevitable feedback delays of a biological motor-control system, is fundamentally limited [10]. Theoretical studies have also shown why modulating the output stiffness of compliant actuators through force-feedback, is not only energetically expensive, but severely limited if the passivity of the overall closed-loop system is to be preserved [53]. While the challenges in providing stable and passive response of feedback controlled dynamical systems can be avoided using open-loop stiffness control, modulating joint stiffness through biological antagonistic actuators is energetically expensive.

[3]This efficiency is lower than the upper bound calculated based on factory specifications $\eta_{\max} = 67\%$ (see Section IV-A).

In the previous section, we showed how to avoid this limitation using a nonbiologically inspired actuator that enables open-loop stiffness modulation with low energy cost. Here, we present experiments to test the suitability of our actuator in low-energy-cost and high-range stiffness augmentation. In these experiments, the actuator was used in parallel to a human to realize a stabilization and a weight-bearing task. We consider these to be two canonical tasks. During the experiments, the behavior of the device was characterized by its output position q, output stiffness K, restoring torque τ, and the motor power p required to modulate or hold the stiffness setting. Human[4] response was quantified through measurement of muscle surface electromyography (EMG) [54].

Raw EMG signals indicate muscle activity; their magnitude is related to the joint torque, joint stiffness, and metabolic power expended by muscles. However, the relation between EMG signals and joint stiffness, torque, and muscle power is nonlinear and challenging to define precisely. In order to provide an estimate of these quantities, the measured EMG signals were processed i.e., rectified, filtered with a 5–100 Hz bandpass filter, and a zero-lag 1 s moving-average filter, and finally normalized. As a first approximation, we assumed that the processed EMG signals corresponded to the two position inputs x_1 and x_2 of the antagonistic actuator shown in Fig. 1(a). Consequently, the stiffness of the human limb, the restoring joint torque, and the muscle power are proportional to: $K \propto x_1 + x_2$, $\tau \propto x_1 - x_2$ and $p \propto (x_1 + x_2)^4$, respectively. These formulas were used to provide a qualitative interpretation of the experimental data in the following way:

1) stiffness is an increasing function of antagonistic muscle coactivation,
2) joint torque depends on the difference of the antagonist and agonist muscle activation, and
3) power is an increasing function of muscle activation.

In the experiments below, we rely on this interpretation to understand the contribution of the human when augmented with the actuator.

A. Postural Stabilization Task

In the following, we report experimental data obtained for two subjects (subject A—female: age 22 year, mass 63 kg, height 1.66 m and subject B–male: age 21 years, mass 88 kg, height 1.80 m). In the first experiment, subjects were asked to keep the inverted pendulum in its unstable vertical configuration [see Fig. 6(a) and (a1)]. The actuator was also connected to the inverted pendulum setup and depending on its stiffness setting, it could help subjects achieve the task.

At the beginning of the experiment ($t \in [33, 53]$ s), the stiffness of the actuator was set to minimum [see Fig. 6(a2) and (a3) black lines]. In this case, the vertical equilibrium of the pendulum was strongly unstable and active involvement of the subjects was required to keep the pendulum in an upright position. This is evident from the EMG recordings [Fig. 6(a2) blue and red lines]. In this case, the task was realized by the human and the energy required by the actuator was low [Fig. 6(a4) black lines].

In the second part of the experiment ($t \in [63, 83]$ s), the stiffness of the actuator was increased until the actuator alone could achieve the task [Fig. 6(a2) and (a3) black lines]. Through this adaptation, the muscle activity of the person [monitored by the EMG recordings Fig. 6(a2)] decreased. When stiffness changed (transient $t \in [53, 63]$ s), the actuator consumed more power [Fig. 6(a4) black lines]. However, holding the stiffness to stabilize the task by the actuator alone required low power. Fig. 6(a3) ($t \approx 63$ s) also shows rapid stiffness change indicating the capability of the actuator to realize fast stiffness modulation at high stiffness settings.

This experiment illustrates how the proposed actuator complements the human when the task is to achieve postural stabilization with low energy cost.

B. Weight-Bearing Task

In the second experiment, the same setup was connected horizontally to a desk [Fig. 6(b)], and subjects were asked to keep the position of the output link fixed. Unlike in the first experiment, here the actuator was operated away from its equilibrium configuration [Fig. 6(b1)], and the task required output torque [Fig. 6(b2) and (b3)]. At the beginning of the experiment ($t \in [0, 23]$ s), the device was set to a high stiffness mode. Under this setting, the output link was deflected due to the effect of gravity. Maintaining this configuration [Fig. 6(b1) dashed lines] required relatively low power by the actuator and minimal involvement by the subject [Fig. 6(b4)].

Subsequently, the stiffness of the device decreased to its minimum value (transient $t \in [23, 33]$ s). When stiffness decreased, keeping the output link at its original position required substantial involvement of the human. In particular, the EMG recordings show higher activation of the agonist (biceps) muscle [Fig. 6(b2) blue and red lines], indicating that fulfillment of this task required torque [Fig. 6(b3)]. This experiment illustrates the ability of the proposed actuator to complement a human by providing stiffness augmentation even if the actuator is deflected from its equilibrium configuration.

In the experiments above, stiffness modulation of the subjects could have emerged due to the mechanical requirement of the task, low confidence level of the human, or due to an unnatural posture of the limb while interacting with the robotic setup. According to Fig. 6(a), (a2), (a3), cocontraction of the muscles emerged while the load imposed on the limb was the same and the posture of the limb did not change, indicating that the observed cocontraction was strongly related to the mechanical requirement of the task. This is because, without substantial involvement of the subject, the considered tasks were not realizable. Despite this, the interaction of the human and the robotic device is complex. For example, the reason for the rapid stiffness adaptation, observed in the stabilization experiment under changing mechanical demands, is not well-understood. Further investigation of this effect requires an extensive human study, which is beyond the scope of this article.

[4]Participants provided written informed consent before the experiment. The study protocol was approved by the Institutional Review Board at the Singapore University of Technology and Design.

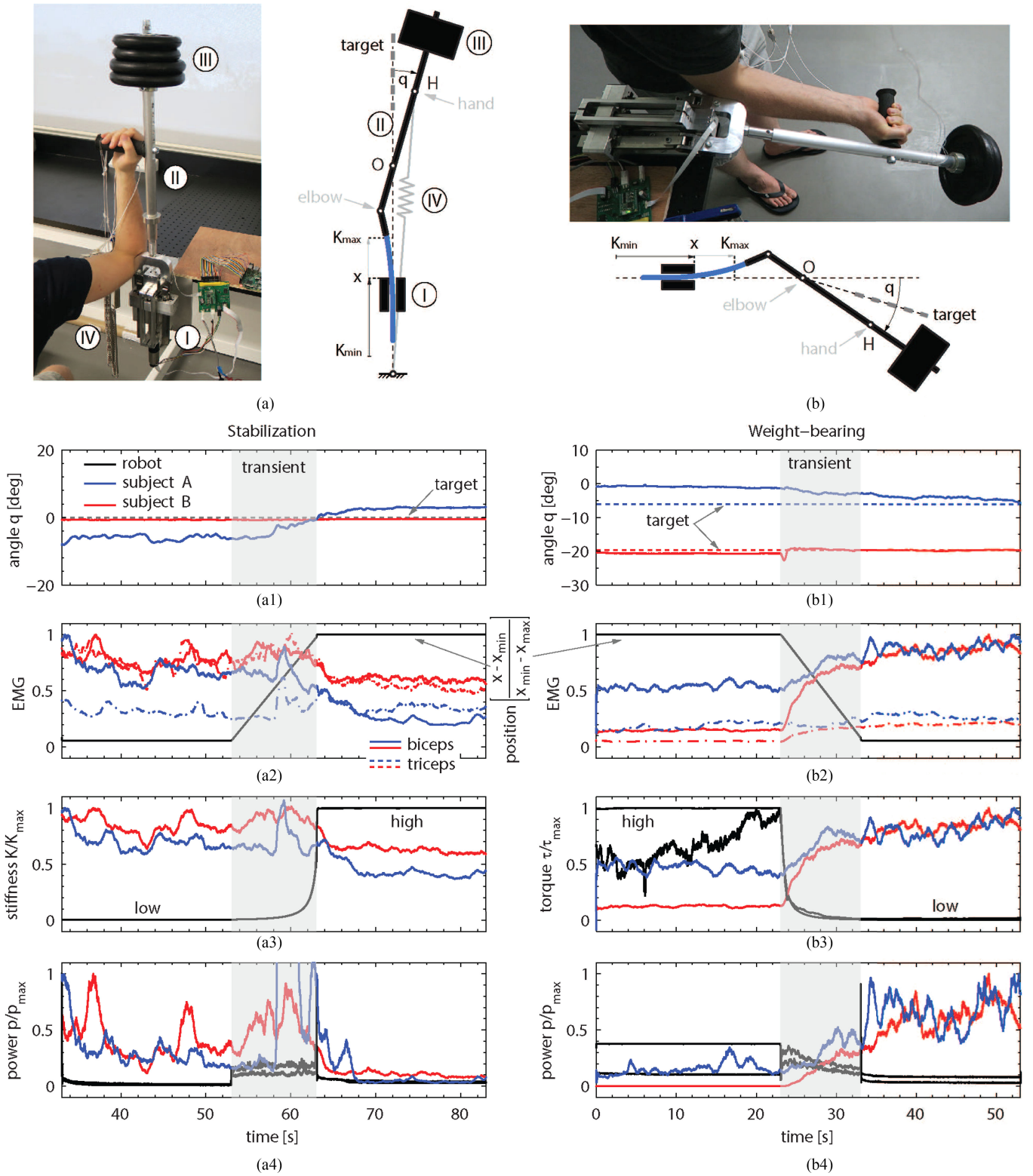

Fig. 6. (a) and (b) Stabilization and weight-bearing tasks. The experiments were performed by two subjects (A and B). Each experiment was repeated five times. The data were subsequently averaged and normalized across the five trials. These data are shown in the plots. (a) Experimental setup for the stabilization task. The setup contains the actuator (I), the link (II) OH=0.4 m, and the mass (III). The mass was 2.5 kg for subject A and 3.75 kg for subject B. The setup was made strongly unstable by the preextended spring (IV) shown with gray. The spring generated a destabilizing negative torsional stiffness (−70 N·m for subject A and −110 N·m for subject B). (b) Experimental setup for the weight-bearing task. This setup did not contain the destabilizing spring. (a1) and (b1) Joint angle (blue and red lines) and the target joint angle (dashed gray, blue, and red lines). (a2) and (b2) Processed biceps (solid lines) and triceps (dashed lines) EMG signals indicating muscle activity during the experiment. The same figure contains the normalized slider position (black lines). (a3) and (b3) Normalized joint stiffness provided by the actuator (black lines) and the human subjects (blue lines). The normalization for the human data is done with respect to the maximum value of the signals excluding the transient (shaded gray area). (a4) and (b4) This plot shows the normalized motor power by the actuator (black lines) and the estimated power by the subjects (blue and red lines).

VI. Conclusion

The idea of human augmentation with robotic devices is not new [55]. Robotic systems designed for this purpose have been developed by many [3], [56]–[58]. The use of control-generated active compliance [59], or passive physical compliance [45], [46], has been recognized as essential in these systems for decades. Compliance is vital to maintain a desirable interaction between the robot and the environment [13], essential to realize a safe human–robot interaction [14], and useful to achieve dynamic behavior [15], [16]. Furthermore, with physical human–machine interaction, it vastly simplifies the coordination of natural and artificial degrees-of-freedom [13]. However, though there have been a number of new developments in this area over the last decade, especially in the design of different types of compliant actuators [19]–[21], it remains challenging to realize effective human augmentation in practical applications.

Series elastic actuators [45] introduce series compliance into the system, a spring placed between the motor unit and the external load, and are capable of modulating the elastic force at the actuator's output using motor position control at its input. These actuators can provide a compliant interface between the robot and the human. This has been recognized as useful in safe human–robot interaction and rehabilitation [60]. These actuators can also store and reutilize elastic energy, and as such enhance power performance over and above what is achievable using rigid actuation [61], [62]. However, series elastic actuators are designed for equilibrium position modulation, and as such, to actively modify the apparent output stiffness, they require closed-loop feedback that can be energetically expensive, and limited by the stability of the controlled system [53].

Variable stiffness actuators [46] are characterized by an open-loop tunable force–displacement relation. In order to provide both equilibrium position and stiffness modulation, these actuators employ motor redundancy and geometric or material nonlinearity by design [43]. For example, by modulating the internal geometry of a variable stiffness design via two position control inputs, these actuators are able to provide a range of equilibrium positions and stiffnesses at their output [15]. However, due to mechanical design, changing the output stiffness of these actuators can be energetically expensive [17], [18]. Furthermore, since these actuators aim to achieve both equilibrium position and stiffness modulation, their design can be more complex, and consequently, less well-suited to develop minimalistic devices aiming to provide human augmentation [1], [23], [48], [63]. Due to these reasons, as of now, the use of variable stiffness actuators for simultaneous equilibrium position and stiffness augmentation remains limited in human augmentation.

In this article, we presented a variable stiffness spring actuator capable of wide-range stiffness modulation with low energy cost. When used in parallel to a human (see Section V), this actuator can provide controllable stiffness augmentation. In this way, it can reduce metabolically expensive muscle coactivation even if it does not provide equilibrium position modulation and does not do net mechanical work. Compared to series elastic actuators, the proposed actuator provides open-loop tunable output stiffness over a large range. In this way, it bypasses stability issues affecting devices that implement closed-loop force control to realize active stiffness modulation. Compared to variable stiffness actuators, the proposed actuator does not provide equilibrium position modulation. Consequently, a variable stiffness spring actuator does not require two motors for redundant actuation and may afford reduced-complexity design realization, essential for controllable autonomous human augmentation.

Examples of reduced-complexity designs of tunable variable stiffness spring actuators have been recently developed [23], [25], [27], [28], [48], [63]. In [48], a fiberglass leaf spring was used to develop a variable stiffness ankle prosthesis that weighs 1 kg (not including battery). In [23], a lightweight 1 kg variable stiffness knee exoskeleton has been developed with on-board power that weighs 1 kg (including battery). In [63], the authors presented a variable stiffness ankle, which weighs less than 1 kg (including battery). These works show how design optimization may enable a compact, wearable, and portable implementation of variable stiffness spring actuators.

Appendix

In this section, we derive the horizontal reaction force in the sliding cantilever support (9). Fig. 7 shows the slider modeled by two parallel plates within a small finite distance Δ. The reaction forces R_1 and R_2 are applied by the slider on the leaf spring, while F_x, F_y, and M are the forces and the moment, which represent part of the beam outside the slider.

In static equilibrium, the following equations hold:

$$\begin{aligned} R_1 - R_2\cos\theta + F_y &= 0 \\ R_2\sin\theta + F_x &= 0 \\ M - R_1 a &= 0 \end{aligned} \tag{24}$$

where θ is the deflection angle of the beam as shown in Fig. 7.

Using the Bernoulli–Euler equation, and assuming that the gap between the two plates is Δ, and the deformation angle θ are small enough to apply small deflection approximation, the relation between the geometry of the support and the reaction forces are given by the following:

$$\Delta = \frac{R_1 a^3}{6EI} = \frac{Ma^2}{6EI}, \quad \theta = \frac{R_1 a^2}{2EI} = \frac{Ma}{2EI}. \tag{25}$$

In order to determine the axial reaction force in the ideal slider support, F_x is calculated as the gap between the two plates Δ tends to zero. Using (24) and (25) under small deflection assumption ($\sin\theta \approx \theta$ and $\cos\theta \approx 1$) we obtain

$$\begin{aligned} F_x &= \lim_{\Delta\to 0} -R_2\sin\theta \approx \lim_{\Delta\to 0} -(R_1 + F_y)\theta \\ &= \lim_{\Delta\to 0} -\left[\frac{M^2}{2EI} + F_y\sqrt{\frac{3M\Delta}{2EI}}\right] = -\frac{M^2}{2EI}. \end{aligned} \tag{26}$$

This relation is used to calculate the dimensionless axial reaction force in the sliding support (9).

Taking the limit $\Delta \to 0$ in (26) allows us to predicts the deformation of the neutral axis, and the forces in the spring. This assumption does not imply that the second area moment I of the spring is zero. The assumption $\Delta \to 0$, together with other standard assumptions used in the Bernoulli–Euler beam theory, make the analytical expressions presented in this article

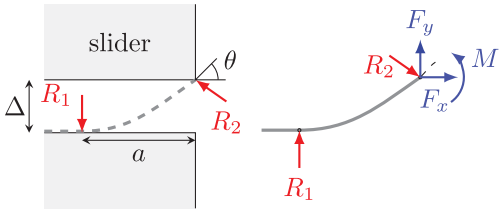

Fig. 7. Local analysis of the forces in the sliding cantilever support.

reasonably simple, but they also make the analytical expressions approximate. For this reason, we used the models to provide qualitative predictions, while we used experiments to verify and quantify these predictions. The experiments are not subject to modeling assumptions.

REFERENCES

[1] S. H. Collins, M. B. Wiggin, and G. S. Sawicki, "Reducing the energy cost of humanwalking using an unpowered exoskeleton," *Nature*, vol. 522, pp. 212–215, 2015.

[2] P. Malcolm, W. Derave, S. Galle, and D. De Clercq, "A simple exoskeleton that assists plantarflexion can reduce the metabolic cost of human walking," *PLoS One*, vol. 8, 2013, Art. no. e56137.

[3] A. M. Dollar and H. Herr, "Lower extremity exoskeletons and active orthoses: Challenges and state-of-the-art," *IEEE Trans. Robot.*, vol. 24, no. 1, pp. 144–158, Feb. 2008.

[4] M. Goldfarb, B. E. Lawson, and A. H. Shultz, "Realizing the promise of robotic leg prostheses," *Sci. Translational Medicine*, vol. 5, no. 210, 2013, Art. no. 210ps15.

[5] H. Lee and N. Hogan, "Time-varying ankle mechanical impedance during human locomotion," *IEEE Trans. Neural Syst. Rehabil. Eng.*, vol. 23, no. 5, pp. 755–764, Sep. 2015.

[6] C. E. English, "Implementation of variable joint stiffness through antagonistic actuation using rolamite springs," *Mechanism Mach. Theory*, vol. 341, pp. 27–40, 1999.

[7] C. E. English and D. Russell, "Mechanics and stiffness limitations of a variable stiffness actuator for use in prosthetic limbs," *Mechanism Mach. Theory*, vol. 341, pp. 7–25, 1999.

[8] S. A. Migliore, E. A. Brown, and S. P. DeWeerth, "Biologically inspired joint stiffness control," in *Proc. IEEE Int. Conf. Robot. Autom.*, Apr. 2005, pp. 4508–4513.

[9] J. W. Hurst, J. E. Chestnutt, and A. A. Rizzi, "The actuator with mechanically adjustable series compliance," *IEEE Trans. Robot.*, vol. 26, no. 4, pp. 597–606, Aug. 2010.

[10] N. Hogan, "Adaptive control of mechanical impedance by coactivation of antagonist muscles," *IEEE Trans. Autom. Control*, vol. AC-29, no. 8, pp. 681–690, Aug. 1984.

[11] D. A. Winter, A. E. Patla, F. Prince, M. Ishac, and K. Gielo-Perczak, "Stiffness control of balance in quiet standing," *J. Neurophysiol.*, vol. 80, pp. 211–1221, 1998.

[12] E. Burdet, R. Osu, D. W. Franklin, T. E. Milner, and M. Kawato, "The central nervous system stabilizes unstable dynamics by learning optimal impedance," *Nature*, vol. 414, pp. 446–449, 2001.

[13] N. Hogan, "Impedance control: An approach to manipulation," *ASME J. Dyn. Syst., Meas. Control*, vol. 107, pp. 1–24, 1985.

[14] A. Bicchi and G. Tonietti, "Fast and soft arm tactics: Dealing with the safety-performance trade-off in robot arms design and control," *IEEE Robot. Automat.. Mag.*, vol. 11, no. 2, pp. 22–33, Jul. 2004.

[15] D. J. Braun, M. Howard, and S. Vijayakumar, "Exploiting variable stiffness in explosive movement tasks," in *Proc. Robot.: Sci. Syst.*, Jun./Jul. 2011, pp. 25–32.

[16] D. J. Braun *et al.*, "Robots driven by compliant actuators: Optimal control under actuation constraints," *IEEE Trans. Robot.*, vol. 29, no. 5, pp. 1085–1101, Oct. 2013.

[17] L. C. Visser, R. Carloni, and S. Stramigioli, "Energy-efficient variable stiffness actuators," *IEEE Trans. Robot.*, vol. 27, no. 5, pp. 865–875, Oct. 2011.

[18] V. Chalvet and D. J. Braun, "Criterion for the design of low power variable stiffness mechanisms," *IEEE Trans. Robot.*, vol. 33, no. 4, pp. 1002–1010, Aug. 2017.

[19] B. Vanderborght *et al.*, "Variable impedance actuators: A review," *Robot. Auton. Syst.*, vol. 61, no. 12, pp. 1601–1614, 2013.

[20] G. Grioli *et al.*, "Variable stiffness actuators: The users point of view," *Int. J. Robot. Res.*, vol. 34, no. 6, pp. 727–743, 2015.

[21] S. Wolf *et al.*, "Variable stiffness actuators: Review on design and components," *IEEE Trans. Mechatronics*, vol. 21, no. 5, pp. 2418–2430, Oct. 2016.

[22] R. Nasiri, A. Ahmadi, and M. N. Ahmadabadi, "Reducing the energy cost of human running using an unpowered exoskeleton," *IEEE Trans. Neural Syst. Rehabil. Eng.*, vol. 26, no. 10, pp. 2026–2032, Oct. 2018.

[23] H. F. Lau, A. Sutrisno, T. H. Chong, and D. J. Braun, "Stiffness modulator: A novel actuator for human augmentation," in *Proc. IEEE Int. Conf. Robot. Automat.*, 2018, vol. 1, pp. 7742–7748.

[24] A. Sutrisno and D. J. Braun, "Enhancing mobility with quasi-passive variable stiffness exoskeletons," *IEEE Trans. Neural Syst. Rehabil. Eng.*, vol. 27, no. 3, pp. 487–496, Mar. 2019.

[25] D. J. Braun, S. Apte, O. Adiyatov, A. Dahiya, and N. Hogan, "Compliant actuation for energy efficient impedance modulation," in *Proc. IEEE Int. Conf. Robot. Automat.*, 2016, pp. 636–641.

[26] T.-H. Chong, V. Chalvet, and D. J. Braun, "Analytical conditions for the design of variable stiffness mechanisms," in *Proc. IEEE Int. Conf. Robot. Automat.*, May 2017, pp. 1241–1247.

[27] A. Dahiya and D. J. Braun, "Efficiently tuneable positive-negative stiffness actuator," in *Proc. IEEE Int. Conf. Robot. Automat.*, May 2017, pp. 1235–1240.

[28] D. J. Braun, V. Chalvet, and A. Dahiya, "Positive-negative stiffness actuators," *IEEE Trans. Robot.*, vol. 35, no. 1, pp. 162–173, Feb. 2019.

[29] J. Choi, S. Hong, W. Lee, S. Kang, and M. Kim, "A robot joint with variable stiffness using leaf springs," *IEEE Trans. Robot.*, vol. 27, no. 2, pp. 229–238, Apr. 2011.

[30] B.-S. Kim and J.-B. Song, "Design and control of a variable stiffness actuator based on adjustable moment arm," *IEEE Trans. Robot.*, vol. 28, no. 5, pp. 1145–1151, Oct. 2012.

[31] A. Jafari, N. G. Tsagarakis, and D. G. Caldwell, "A novel intrinsically energy efficient actuator with adjustable stiffness (AwAS)," *IEEE/ASME Trans. Mechatronics*, vol. 18, no. 1, pp. 355–365, Feb. 2013.

[32] A. Jafari, N. G. Tsagarakis, I. Sardellitti, and D. G. Caldwell, "A new actuator with adjustable stiffness based on a variable ratio lever mechanism," *IEEE/ASME Trans. Mechatronics*, vol. 19, no. 1, pp. 55–63, Feb. 2014.

[33] R. Van Ham, B. Vanderborght, M. Van Damme, B. Verrelst, and D. Lefeber, "MACCEPA: The mechanically adjustable compliance and controllable equilibrium position actuator: Design and implementation in a biped robot," *Robot. Auton. Syst.*, vol. 55, no. 10, pp. 761–768, 2007.

[34] S. Wolf and G. Hirzinger, "A new variable stiffness design: Matching requirements of the next robot generation," in *Proc. IEEE Int. Conf. Rob. Automat.*, 2008, pp. 1741–1746.

[35] S. S. Groothuis, G. Rusticelli, A. Zucchelli, S. Stramigioli, and R. Carloni, "The variable stiffness actuator vsaUT-II: Mechanical design, modeling, and identification," *IEEE/ASME Trans. Mechatronics*, vol. 19, no. 2, pp. 589–597, Apr. 2014.

[36] S. Groothuis, R. Carloni, and S. Stramigioli, "A novel variable stiffness mechanism capable of an infinite stiffness range and unlimited decoupled output motion," *Actuators*, vol. 3, no. 2, pp. 107–123, 2014.

[37] G. Mathijssen, D. Lefeber, and B. Vanderborght, "Variable recruitment of parallel elastic elements: Series–parallel elastic actuators (SPEA) with dephased mutilated gears," *IEEE Trans. Mechatronics*, vol. 20, no. 2, pp. 594–602, Apr. 2015.

[38] T. Morita and S. Sugano, "Design and development of a new robot joint using a mechanical impedance adjuster," in *Proc. IEEE Int. Conf. Robot. Automat.*, May 1995, vol. 3, pp. 2469–2475.

[39] T. Morita and S. Sugano, "Development of one-DOF robot arm equipped with mechanical impedance adjuster," in *Proc. IEEE Int. Conf. Intell. Robots Syst.*, Aug. 1995, pp. 407–412.

[40] T. Morita and S. Sugano, "Development of 4-DOF manipulator using mechanical impedance adjuster," in *Proc. IEEE Int. Conf. Robot. Automat.*, Apr. 1996, pp. 2902–2907.

[41] T. Morita and S. Sugano, "Development of an anthropomorphic force-controlled manipulator WAM-10," in *Proc. Int. Conf. Adv. Robot.*, Jul. 1997, pp. 701–706.

[42] F. Petit, M. Chalon, W. Friedl, M. Grebenstein, A. Albu-Schaffer, and G. Hirzinger, "Bidirectional antagonistic variable stiffness actuation: Analysis, design and implementation," in *Proc. IEEE Int. Conf. Robot. Automat.*, May 2010, pp. 4189–4196.

[43] K. F. Laurin-Kovitz, J. E. Colgate, and S. D. R. Carnes, "Design of components for programmable passive impedance," in *Proc. IEEE Int. Conf. Robot. Automat.*, 1991, vol. 2, pp. 1476–1481.
[44] T. Sugar and K. Hollander, "Adjustable stiffness leaf spring actuators," U.S. Patent 7 527 253 B2, 2009.
[45] G. Pratt and M. Williamson, "Series elastic actuators," in *Proc. IEEE/RSJ Int. Conf. Intell. Robots Syst.*, 1995, vol. 1, pp. 399–406.
[46] R. van Ham, T. Sugar, B. Vanderborght, K. Hollander, and D. Lefeber, "Compliant actuator designs," *IEEE Robot. Automat. Mag.*, vol. 16, no. 3, pp. 81–94, Sep. 2009.
[47] D. J. Braun, "Optimal parametric feedback excitation of nonlinear oscillators," *Phys. Rev. Lett.*, vol. 116, 2016, Art. no. 044102.
[48] M. K. Shepherd, and E. J. Rouse, "Design of a quasi-passive ankle-foot prosthesis with biomimetic, variable stiffness," in *Proc. IEEE Int. Conf. Robot. Automat.*, May 2017, pp. 6672–6678.
[49] S. Diller, C. Majidi, and S. H. Collins, "A lightweight, low-power electroadhesive clutch and spring for exoskeleton actuation," in *Proc. IEEE Int. Conf. Robot. Automat.*, May 2016, pp. 682–689.
[50] S. Seok *et al.*, "Design principles for energy-efficient legged locomotion and implementation on the MIT cheetah robot," *IEEE/ASME Trans. Mechatronics*, vol. 20, no. 3, pp. 1117–1129, Jun. 2015.
[51] B. Whipp and K. Wasserman, "Efficiency of muscular work," *J. Appl. Physiol.*, vol. 26, pp. 644–648, 1969.
[52] V. Chalvet and D. J. Braun, "Algorithmic design of low power variable stiffness mechanisms," *IEEE Trans. Robot.*, vol. 33, no. 6, pp. 1508–1515, Jun. 2017.
[53] J. E. Colgate and N. Hogan, "Robust control of dynamically interacting systems," *Int. J. Control*, vol. 48, no. 1, pp. 65–88, 1988.
[54] C. I. DeLuca, "The use of surface electromyography in biomechanics," *J. Appl. Biomech.*, vol. 13, no. 2, pp. 135–163, 1997.
[55] N. Yagn, "Apparatus for facilitating walking, running, and jumping," U.S. Patents 420 179 and 438 830, 1890.
[56] B. R. Fick and J. B. Makinson, "Hardiman I prototype for machine augmentation of human strength and endurance," General Electric Company, Schenectady, NY, Research and DevelopmentTech. Rep. S-71-1056, 1971.
[57] M. Vukobratović, D. Hristić, and Z. Stojiljković, "Development of active anthropomorphic exoskeletons," *Med. Biol. Eng.*, vol. 12, no. 1, pp. 66–80, 1974.
[58] A. J. Young and D. P. Ferris, "State of the art and future directions for lower limb robotic exoskeletons," *IEEE Trans. Neural Syst. Rehabil. Eng.*, vol. 25, no. 2, pp. 171–182, Feb. 2017.
[59] K. J. Salisbury, "Active stiffness control of a manipulator in cartesian coordinates," in *Proc. IEEE Conf. Decis. Control*, Dec. 1980, vol. 19, pp. 95–100.
[60] H. Vallery, J. Veneman, E. V. Asseldonk, R. Ekkelenkamp, M. Buss, and H. V. D. Kooij, "Compliant actuation of rehabilitation robots," *IEEE Robot. Automat. Mag.*, vol. 15, no. 3, pp. 60–69, Sep. 2008.
[61] D. Paluska and H. Herr, "The effect of series elasticity on actuator power and work output: implications for robotic and prosthetic joint design," *Robot. Auton. Syst.*, vol. 54, no. 8, pp. 667–673, 2006.
[62] D. W. Haldane, M. M. Plecnik, J. K. Yim, and R. S. Fearing, "Robotic vertical jumping agility via series-elastic power modulation," *Sci. Robot.*, vol. 1, no. 1, 2016, Art. no. eaag2048.
[63] E. M. Glanzer and P. G. Adamczyk, "Design and validation of a semi-active variable stiffness foot prosthesis," *IEEE Trans. Neural Syst. Rehabil. Eng.*, vol. 26, no. 12, pp. 2351–2359, Dec. 2018.

David J. Braun (M'09) received the Ph.D. degree in mechanical engineering from Vanderbilt University, Nashville, TN, USA, in 2009.

He is currently an Assistant Professor of Mechanical Engineering with Vanderbilt University (VU). Prior to joining VU, he was a Research Associate with the Center for Intelligent Mechatronics, VU, a Visiting Researcher with the Institute for Robotics and Mechatronics, German Aerospace Center, Cologne, Germany, a Postdoctoral Research Fellow with the Statistical Machine Learning and Motor Control Group, University of Edinburgh, Edinburgh, Scotland, and an Assistant Professor with Singapore University of Technology and Design, Singapore. His research interests include dynamical systems, optimal control, and robotics.

Dr. Braun was a recipient of the 2013 IEEE Transactions on Robotics Best Paper Award. He was a Scientific Program Co-Chair of the 2015 IEEE International Conference on Rehabilitation Robotics, and an Area Chair for the 2018 Robotics Science and Systems Conference.

Vincent Chalvet received the engineering degree in mechatronics from École Nationale Supérieure de Mécanique et des Microtechniques, Besançon, France, in 2008, and the Ph.D. degree in automatic control from Franche-Comte University, Besancon, France, in 2013.

He spent two years as a Postdoctoral Research Fellow with Singapore University of Technology and Design working on the design of energy-efficient compliant robotic actuators. He is currently a Postdoctoral fellow at ENSTA Paris, Palaiseau, France, working on decision making for autonomous vehicles. His research interest includes robotics from design to control.

Tze-Hao Chong received the M.S. degree in robotics systems development from Robotics Institute, Carnegie Mellon University, Pittsburgh, PA, USA, in 2018, and the B.Eng. degree in engineering product development from the Singapore University of Technology and Design, Singapore, in 2015.

Prior to his M.S studies, he was a Research Assistant with the Singapore University of Technology and Design, where he worked on variable stiffness mechanisms and embedded software. He is now a Software Engineer with the Open Source Robotics Foundation. He works on the Robotics Middleware Framework intended for the healthcare industry in Singapore. His research interests include robotics, computer vision, and machine learning.

Salil S. Apte received the B.S. (Hons.) degree in mechanical engineering from IIT Kharagpur, Kharagpur, India, in 2013, and the M.S. degree in mechanical engineering (*cum laude* and Hons.) from TU Delft, Delft, The Netherlands, in 2017. He is currently working toward the doctoral degree under the Robotics, Control, and Intelligent Systems Program at EPFL, Lausanne, Switzerland.

Prior to his doctoral studies, he was a Researcher with the BioRobotics Lab, TU Delft, the Dynamics & Control Laboratory, Singapore University of Technology and Design, Singapore, and the Energy Biosciences Institute, University of California, Berkeley, Berkeley, CA, USA, where he worked on dynamical modeling and in-lab analysis of human gait for neuro-rehabilitation, design and development of energy-efficient compliant actuators, and mechanical modeling of plant cell walls, respectively. He is a EPFLinnovators fellow. His research interests include signal processing, sensor fusion, human-robot interaction, and rehabilitation engineering, with an emphasis on the biomechanics of human locomotion, currently he focuses in-field measurement of human motion using wearable sensors, with the goal of optimizing training in sports and rehabilitation.

Neville Hogan received the Diploma in engineering (with distinction) from Dublin Institute of Technology, Dublin, Ireland, in 1970, the M.S. degree in mechanical engineering from Massachusetts Institute of Technology (MIT), Cambridge, MA, USA, in 1973, and the Ph.D. degree from MIT, in 1977.

He is Sun Jae Professor of Mechanical Engineering and Professor of Brain and Cognitive Sciences with the MIT. He joined MIT's faculty in 1979 and currently directs the Newman Laboratory for Biomechanics and Human Rehabilitation, Cambridge, MA, USA. He cofounded Interactive Motion Technologies, now part of Bionik Laboratories. His research interests includes robotics, motor neuroscience, and rehabilitation engineering, emphasizing the control of physical contact and dynamic interaction.

Dr. Hogan is a recipient of the following awards: Honorary Doctorates from Delft University of Technology and Dublin Institute of Technology; the Silver Medal of the Royal Academy of Medicine in Ireland; the Henry M. Paynter Outstanding Investigator Award and the Rufus T. Oldenburger Medal from the American Society of Mechanical Engineers, Dynamic Systems and Control Division; and the Academic Career Achievement Award from the Institute of Electrical and Electronics Engineers, Engineering in Medicine and Biology Society.